

# **Anatomic and Neurochemical Studies of the Human Ventral Medulla in Early Life**

## **Observations Relevant to the Sudden Infant Death Syndrome**

**HANNAH C. KINNEY, J. J. FILIANO,  
A. PANIGRAPHY, and L. A. RAVA**

Harvard Medical School and Children's  
Hospital  
Boston, Massachusetts

**W. F. WHITE**

Pfizer, Inc.  
Groton, Connecticut

### **I. Introduction**

This report highlights work in our laboratory related to the possible role of the ventral medulla in the sudden infant death syndrome (SIDS). SIDS is the leading cause of postneonatal infant mortality in the United States today, causing approximately 7000 deaths/year (1). It is defined as the sudden death of an infant under 1 year of age that remains unexplained after a thorough case investigation, including a complete autopsy (1). Typically, SIDS is a sleep-related sudden death. Ninety percent of the deaths occur within the first 6 months of life, with a peak at 2 to 4 months. This unique and consistent age distribution suggests that, while the causes of SIDS may be heterogeneous, there is likely a final common pathway that is related to a critical period in development (2). We have proposed a triple-risk model for the pathogenesis of SIDS in which sudden death results from the intersection of three key factors: (a) an infant made vulnerable by an underlying abnormality in the control of homeostasis during sleep; (b) a critical developmental period in homeostasis and state of maturation, i.e., the first 6 months of life, as the newborn makes the transition to extrauterine life; and (c) an exogenous stressor, such as infection or

overheating secondary to swaddling (3). A variety of autonomic irregularities have been reported in infants who subsequently die of SIDS, strengthening the possibility of a primary defect in autonomic and/or respiratory regulation (2). Many of these differences become apparent only during particular sleep-waking states, further suggesting central neural dysfunction (2). Maternal risk factors for SIDS (e.g., cigarette smoking during pregnancy) suggest that the intrauterine environment is suboptimal, with the implication that the pathogenesis of SIDS begins before birth (2). Subtle neurological dysfunction at birth in future SIDS victims supports the idea of pre- and/or perinatal brain injury (2).

In its broadest terms, our driving hypothesis is that SIDS, or a subset of SIDS, results from a defect in an appropriate response to a life-threatening challenge during sleep, e.g., asphyxia or hypercarbia, as the infant passes through the critical developmental period (2). A major anatomic site relevant to this hypothesis is the ventral medulla, a region critical for the integration of autonomic function, ventilation, chemoreception, and arousal (4-15). This region contains neuronal and glial cells along the surface known as the respiratory chemosensitive fields (RCF) (5,7-15). Experiments in cats and in medulla slice preparations from cats identify CO<sub>2</sub> and hydrogen ion responsive neuronal and glial populations at the RCF, which many investigators believe mediate ventilatory and behavioral responses to CO<sub>2</sub> and hydrogen ion (5,7-15). SIDS, or a subset of SIDS, may be due to a defect in neurons of the ventral surface of the medulla, resulting in an impaired response to a hypercarbic challenge during sleep that leads to a cascade of progressive hypercarbia, CO<sub>2</sub> necrosis, impaired airway reflexes, and ultimately, sudden death (16). The concept that a primary defect in ventral medullary surface (VMS) neurons may be involved in the pathogenesis of SIDS is supported by epidemiologic data indicating that the risk for SIDS is increased in infants sleeping prone, a position that is postulated to result in asphyxia or CO<sub>2</sub> rebreathing when the head is face-down (17-20). Moreover, recent clinical data indicate that some infants do sleep in the face-down position and that this position results in increased end-tidal PCO<sub>2</sub> (20). An infant with a primary VMS defect may be vulnerable to sudden death by rebreathing CO<sub>2</sub> in the prone position during sleep, particularly when stressed by even a minor infection and during a critical period in the maturation of respiratory and other homeostatic control systems during sleep.

In the following report, we first review anatomic evidence that the human arcuate nucleus (ARC) is homologous to a cell population in the cat VMS considered responsive to CO<sub>2</sub>, and, second, consider evidence for a severe, developmentally related anatomic deficiency, or hypoplasia, in a subset of SIDS victims. We then provide baseline data about neurotransmitter receptor binding in the ARC and selected cardioventilatory-related nuclei of the developing human medulla that are relevant to neurochemical analysis in SIDS brainstems.

## II. Anatomic Studies of the Human Infant VMS

The morphology and topographic distribution of the central chemosensors in the human medulla are not known definitively. This is because the physiological experiments required for their direct identification, namely lesion studies or stimulation by acidic solutions or electrical current, are prohibitive in humans. The only distinct neuronal population along the human VMS itself is the ARC, which historically has been considered a relay nucleus from the cerebral cortex to the cerebellum via the external arcuate fibers and inferior cerebellar peduncle (21,22). In a comparative anatomic study between the human infant and cat VMS, we found that the ARC, nucleus (n.) conterminalis, and foci of thickened marginal glia (TMG) in the human are anatomically homologous to the cat RCF (Table 1) (23). This homology is based upon cytoarchitectonic criteria (including cell size, shape, and distance from the surface) as defined in the combined neuroanatomic and physiological studies of the cat RCF of Trouth, Schläfke, and others (11-14,23), and upon three-dimensional cell distributions, as determined with the aid of computer reconstructions (23). The human n. conterminalis, located in the caudal ventrolateral medulla, is composed of large fusiform or multipolar cells that are cytologically identical to those described by Trouth et al. in the cat L field (11-13,23). In contrast to humans, however, the cells in cats do not form a distinct nucleus, but rather cluster in groups of two to three. The large, fusiform neurons described by Trouth et al. are present in ventrolateral and dorsomedial clusters extending the length of the twelfth cranial nerve (CN 12) roots, with the ventrolateral clusters matching most closely the distribution of the L field (11-13). Homologous ventrolateral neurons of the n. conterminalis and associated TMG comprise the caudal putative RCF in the human infant (Table 1). In contrast to cats, however, in humans the CN 12 extends almost the entire length of the medulla and does not demarcate the rostral boundary of the caudal RCF.

The human ARC is anatomically homologous to a second neuronal population on the cat VMS composed of smaller neurons located along the entire caudorostral length of the medulla (Table 1). In cats and humans, these neurons are small, round or oval, with indistinct Nissl substance. In cats they occur in clusters of two to four, compared to larger clusters of ten or more in humans. In humans, there are a large number of ARC neurons in the midline, but such midline cells are not shown within the experimentally determined RCF because the caudal position of the basilar artery makes this locus inaccessible in cats (23). The midline ARC is homologous to the small cells located at the ventral aspect of the cat n. raphe pallidus. In cats, the ventrolateral small round neurons and associated TMG occupy the rostral region corresponding to the S and M fields, whose distribution is marked by the roots of CN 9, 10, and 7. Homologous ARC neurons and TMG comprise the rostral putative human RCF;

**Table 1** Anatomic Homology in Neuronal Cell Populations of the Ventral Medullary Surface Between the Cat and Human Infant<sup>a</sup>

Species	Nucleus/RCF	Neuron type	Neuron size, microns (SD)	Distance from surface of medulla, microns (SD)	Caudal-to-rostral distribution of cells
Cat	M and S RCF	Small, round	L = 16 (3) W = 11 (2)	284 (95)	Caudal medulla to caudal pons
Human	Arcuate nucleus	Small, round	L = 15 (3) W = 10 (2)	180 (83)	Caudal medulla to merge with basis pontis
Cat	L RCF	Large, fusiform	L = 31 (10) W = 11 (3)	406 (258)	From caudal to rostral extent of CN 12 roots
Human	N. conterminalis	Large, fusiform	L = 28 (6) W = 14 (3)	1003 (273)	From caudal to middle extent of medulla/CN 12 roots

Source: Ref. 23.

<sup>a</sup>Small, round neurons and large, fusiform neurons occasionally intermingle in caudal regions in both cat and human infant medullas. The neurons of the human n. conterminalis are deeper from the surface than large, fusiform cells (Trough) in the cat caudal RCF; this reflects, in part, the merging of a large number of conterminalis cells with the n. raphe pallidus and medial olivary nucleus. Abbreviations: L, length; W, width; SD, standard deviation.

the landmarks of the rostral RCF are the roots of CN 9, 10, and 7, as in cats. Of note, ARC neurons extend the entire length of the human infant medulla and are probably part of the caudal as well as rostral human RCF.

A role for the ARC in vital functions is based on anatomic and physiological evidence from experimental animals and human clinicopathological correlations (15,16,24). The ablation of neurons in animals in sites homologous to the human ARC produces apnea and/or reduces blood pressure, depending on the precise site lesioned (16). Neurons in homologous positions to those of the ARC project to several nuclei related to ventilatory and autonomic regulation in the brainstem and spinal cord (16). A role for the ARC in human ventilatory control is supported by the report of its absence in an autopsied 5-month-old infant with congenital central hypoventilation syndrome (24). The human ARC is also known to project to the cerebellum (25), suggesting that it may link an autonomic/chemosensory/arousal integration zone of the ventral medulla to that structure. Further characterization of the neurochemistry, ultrastructure, connectivity, and physiological activity of the ARC and the small cells of the cat VMS is needed to confirm or refute their homology and to understand their function better.

### III. An Anatomic Study of the ARC in SIDS Victims

Having identified the ARC as a putative component of the VMS cell populations related to central chemoreception, we next asked the question: Is there an anatomic deficiency of the ARC in SIDS victims? To address this question, we surveyed serially or extensively sectioned medullas of 41 SIDS victims and 27 controls in a blinded fashion. We identified two cases in which the ARC was almost totally absent; after breaking the code, we found that both cases were SIDS victims (16). Three-dimensional reconstructions and volume measurements were performed in serial sections from one of these SIDS victims and from three infant controls: the volume of the right ARC nucleus in the SIDS case was 0.7 mm<sup>3</sup>, compared to a range of 3 to 26 mm<sup>3</sup> (median, 5 mm<sup>3</sup>) in the three controls. This study suggested that ARC hypoplasia characterizes at least a subset of SIDS victims [2/41 SIDS victims (5%)] (16). Based upon the known anatomic connections of the human ARC and the connections and functions of neurons in homologous positions in experimental animals, we postulate that ARC hypoplasia may lead to sudden death in at least some SIDS victims by dyssynergy between autonomic, chemosensory, and arousal integration and the cerebellar coordination of ventilation, especially during sleep and hypercarbia in a critical developmental period (16).

A major question in the two SIDS cases with ARC hypoplasia concerns the mechanism whereby a congenital lesion in the ARC does not cause clinically apparent autonomic and ventilatory disturbances in the neonatal period but leads to death in the postneonatal period (16). The answer to this question is

unknown but may be related to the same or similar mechanisms that underlie the age-related aspects of SIDS in general (2,16). Infants with ARC hypoplasia may be at particular risk for SIDS because, without the full complement of neurons and/or neuropils in the VMS cell populations, they are unable to make age-appropriate transitions in cardioventilatory and/or arousal control during the critical developmental period (2,16). Moreover, exogenous stressors may tip an already precarious balance. Of note, exogenous stressors associated with SIDS tend to cause hypercarbia, alter the demand for cardiac output and/or thermoregulation, and/or decrease arousal. These factors include infection, fever, environmentally induced hyperthermia, and bedding that traps the infant's face in an air pocket and results in rebreathing (17–20). The cause of the ARC hypoplasia in the two SIDS victims of the anatomic study is unknown. There were no other brainstem anomalies, nor was there gliosis or apparent neuronal atrophy within the ARC that would suggest a destructive or degenerative process (16). Given the timing and pattern of the formation of the human ARC from the rhombic lip (25), we speculate that the hypoplasia is restricted to rhombic lip precursors destined to differentiate into ARC neurons. Genetic or toxic insults to the regulation of ARC neuronal number during the first 16 weeks of pregnancy are considerations (16).

#### IV. A Baseline Study of Neurotransmitter Receptor Binding in Cardioventilatory-Related Nuclei of the Developing Human Medulla

ARC hypoplasia may characterize a small subset of SIDS victims with a putative primary defect in central chemoreception. Alternatively, this anatomic deficiency may represent the severe end of a spectrum of ARC abnormalities in a wider SIDS group, with neurochemical or molecular abnormalities (not detectable with the light microscope) at the more subtle end (16). To explore the possibility of a neurochemical deficiency in the ARC in SIDS victims, we have chosen to examine the parameter of neurotransmitter receptor binding with tissue autoradiography. A major strength of tissue receptor autoradiography is that it provides information about possible neurotransmitter abnormalities in nuclei that are histologically unremarkable, a major consideration in the analysis of SIDS brainstems (2). This technique also allows for the localization of neurotransmitter receptor binding within precisely defined anatomic loci, even the small size of the human ARC on individual sections. In addition, it allows for analysis of all nuclei, such that an isolated defect in receptor binding in the ARC may be detected by the comparison of measurements between other nuclei as well as the ARC. Yet virtually nothing is known about neurotransmitter receptor binding in the human ARC, especially its developmental profile across early life. Thus, as a first step toward the comparative analysis of neurotransmitter receptor binding in the ARC of SIDS victims and

controls, we performed a baseline study in control cases without SIDS or clinical neurological disease. We selected radioligands that bind to the receptors of neurotransmitters implicated in mediating VMS cell responses in experimental animals—e.g., muscarinic, nicotinic, opioid, and kainate (KA) receptors (10, 26–34). We also selected radioligands that bind to all or many of the subtypes of a particular receptor: given the paucity of information about neurotransmitter receptor binding in the developing human ARC in general, our initial aim is to provide baseline data about the quantitative distribution of the major subtypes combined.

#### A. Materials and Methods

The specimens analyzed in this study were part of a database under development in our laboratory for delineating brainstem chemical anatomy in early human life in relationship to the SIDS problem (35–40). Brainstems were obtained from individuals with postmortem intervals  $\leq 24$  h. Age is expressed as post-conceptual (gestational plus postnatal) weeks. The fetal specimens at mid-gestation were obtained from elective abortuses autopsied in the Department of Pathology, Brigham and Women's Hospital, Boston, Massachusetts, with approval of the Clinical Protection Committee. Fetal age was determined by foot length measurements.

Quantitative receptor autoradiography was performed in frozen human fetal and infant medullas based upon methods developed in experimental animals or adult human postmortem tissues (Table 2) (35–46). Our procedures for tissue preparation and sampling have been described in detail (35). Brainstem sections from each case were incubated with different radioligands for comparison of muscarinic cholinergic, nicotinic cholinergic, opioid, serotonergic (5HT),  $\alpha_2$ -adrenergic, and KA receptor binding patterns. In a sample of adjacent serial-sections from each case, the following radioligands were applied:  $^3\text{H}$ -quinuclidinyl benzilate (QNB) for muscarinic cholinergic receptor (mAChR) binding;  $^3\text{H}$ -nicotine for nicotinic cholinergic receptor (nAChR) binding (39,45);  $^3\text{H}$ -naloxone for opioid binding (35);  $^3\text{H}$ -lysergic acid diethylamide for 5HT binding (38,42);  $^3\text{H}$ -para-aminoclonidine (PAC) for  $\alpha_2$ -adrenergic binding (43,44); and  $^3\text{H}$ -KA for KA binding (40,46) (Table 2). Nonspecific binding was determined with appropriate displacers (Table 2). Our procedures for washing and drying the sections and generating the autoradiograms have been previously described (35,37). Sections were exposed to  $^3\text{H}$ -sensitive film (LKB Ultrofilm- $^3\text{H}$ ) for 8 to 24 weeks (Table 2).

In this baseline study, we measured neurotransmitter receptor binding in the ARC, n. tractus solitarii (nTS), and n. paragigantocellularis lateralis (PGL). The nTS, a vagal subnucleus, is a major site of cardioventilatory reflex integration: it receives afferent information from mechano-, irritant, baro-, and peripheral and central chemoreceptors; bulbospinal neurons of the dorsal respiratory group colocalize with the nTS and drive spinal cord motor neurons

**Table 2** Experimental Conditions for Neurotransmitter Receptor Binding

Receptor	Ligand	Putative binding sites	Displacer	Preincubation buffer	Incubation buffer	Incubate (min)	Expose (weeks)
Muscarinic	<sup>3</sup> H-QNB 1 nM	m1-m5	Atropine sulfate 1 μM	NaH <sub>2</sub> PO <sub>4</sub> 50 nM NaCl 100 mM 30 min	NaH <sub>3</sub> PO <sub>4</sub> 50 nM NaCl 100 mM	120	8
Nicotinic	<sup>3</sup> H-D,L-Nicotine 3.5 nM	α <sub>4</sub> β <sub>2</sub>	L-Nicotine bitartrate 10 μM	None	Tris-HCl 50 mM	20	12
5HT	<sup>3</sup> H-LSD 5 nM	5HT (5HT <sub>1c</sub> ) 5HT <sub>2</sub>	Serotonin 100 μM	TRIS-maleate 300 mM pH 7.4	CaCl <sub>2</sub> 8 mM Tris-maleate 300 mM, pH 7.4, ascorbic acid 0.1%	60	8
KA	<sup>3</sup> H-KA 4 nM	High affinity: GluR5- GluR7, KA1, KA2 Low affinity: GluR1- GluR4	KA 100 μM	Tris-HCl 50 mM pH 7.4 30 min	Tris-HCl 50 mM pH 7.4 4°C	60	24
Opioid	<sup>3</sup> H-Naloxone 2 nM	All major subtypes: mu > kappa > delta	5 μM Naloxone	Tris HCl 50 mM 30 min	Tris-HCl	60	10
α-2	<sup>3</sup> H-PAC 1 nM phenotolamine	High affinity: α <sub>2</sub>	10 μM phenotol- amine	NaH <sub>2</sub> PO <sub>4</sub> 50 mM EDTA 10 mM 20 min	Tris-HCl 170 mM MgCl <sub>2</sub> 10 mM	60	12

Source: Refs. 35, 37-46, 51.

projecting to respiratory muscles (47). The nTS also projects to ventrolateral medulla sites integral to blood pressure regulation. The PGL, located in the ventrolateral reticular formation of the rostral medulla, is a putative integrative site of respiratory drive inputs and a candidate site for the rostral vasomotor control area (9). Measurements in the ARC were made in two sections from six precisely defined levels from each case; the nTS measurement was made at one midmedullary level, and PGL measurements at two rostral medulla levels. Plates in the atlas of Olszewski and Baxter (21) were used for reference. The six levels, with their atlas plate numbers (21), were: (a) caudal medulla, level of n. gracilis (Plate VIII); (b) caudal medulla, level of area postrema (Plate X); (c) midmedulla, level of n. Roller (Plate XII) (nTS measurement); (d) rostral medulla, level of n. praepositus (Plate XIV) (PGL measurement); (e) rostral medulla, level of n. vestibularis spinalis (Plate XVI) (PGL measurement); and (f) rostral medulla, level of rostral pole of principal inferior olive (Plate XVIII). In order to define the anatomic boundaries of brainstem nuclei, the tissue sections that generated the autoradiograms were stained with cresyl violet or hematoxylin and eosin and compared with the autoradiogram.

Quantitative densitometry of autoradiographs was performed with a MCID imaging system (Imaging Research Inc., Ontario). Optical densities were converted to specific activities in femtomoles/milligram (fmoles/mg) tissue with <sup>3</sup>H-standards. Receptor density was determined in specific nuclei by digitizing the nuclear boundaries directly upon the specific activity mosaic displayed on the color monitor, with superimposition of the cell-stained tissue section over the specific activity mosaic, when necessary, with software available on the imaging system. Specific activity measurements were made in a blinded fashion, without knowledge of clinical diagnosis or postconceptional age. Receptor density values from right and left paired nuclei were combined as significant differences between them were not found, and were expressed as the mean. Specific activity data were displayed as computer-generated mosaics with a linear, 15-step gray scale. The range varied depending upon the specific radioligand used. A *t*-test was used to compare radioligand binding between the fetal and infant groups.

Because tissue receptor autoradiography with tritiated ligands is subject to differential quenching by varying lipid levels in the tissue, we considered the possibility that increased lipid quench due to progression of brainstem myelination explains developmental changes in binding to the selected tritiated radioligands (37,48). To test this possibility, we corrected tritiated radioligand binding for quench using <sup>3</sup>H-succinidyl proprionate (SP) (37,49). The brainstem sections used for <sup>3</sup>H-SP binding were adjacent to those in which binding was examined. <sup>3</sup>H-SP activity before and after delipidation was compared in the same tissue sections using the MCID system: the autoradiograms of the same tissue sections before and after delipidation were aligned with one another, and measurements of <sup>3</sup>H-SP binding were made within the identical anatomic boundaries of the selected nuclei (37). We tested the effect of quench in

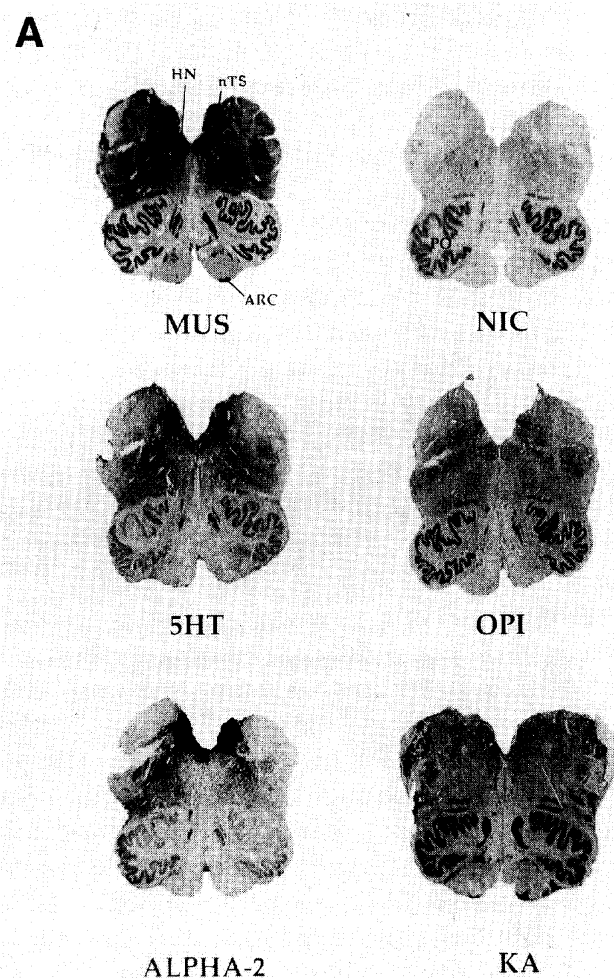
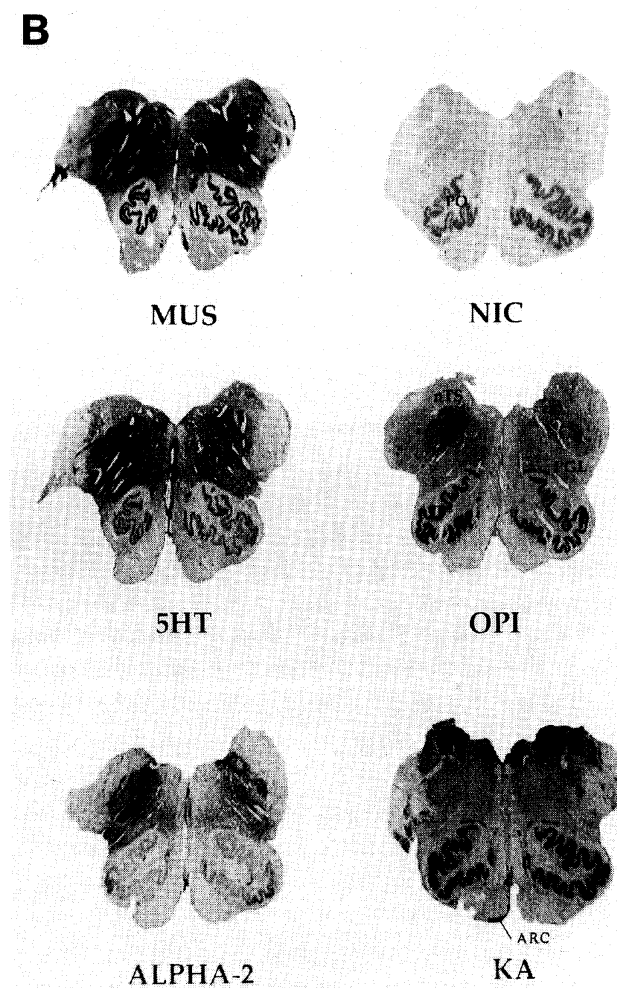


**Figure 1** (A) The distribution of neurotransmitter receptor binding using six radioligands (Table 2) in the midmedulla (level of the n. Roller) and (B) rostral medulla (level of the n. prepositus) in a representative infant at 52 postconceptional weeks. As KA binding was not available in this case, it is illustrated from the medulla of a 47-postconceptional-week infant. Each image represents a specific activity mosaic in which the range of binding is illustrated by a linear 15-step gray scale. (Note that the range varies for each radioligand—e.g., 0 to 50 fmol/mg for  $^3\text{H}$ -KA binding to KA receptors, 0 to 240 fmol/mg for  $^3\text{H}$ -QNB binding to mAChRs). Abbreviations: MUS, muscarinic; NIC, nicotinic; 5HT, serotonergic; OPI, opioid; alpha,  $\alpha_2$ -adrenergic; KA, kainate; ARC, arcuate nucleus; nTS, n. tractus solitarius; PGL, n. paragigantocellularis; PO, principal inferior olive.



selected nuclei by dividing specific activity of binding by efficiency ( $^3\text{H}$ -SP binding before delipidation divided by  $^3\text{H}$ -SP binding after delipidation) (37,49).

### B. Results

In this baseline study, we examined radioligand binding to the selected neurotransmitter receptors in a total of 20 cases. The brainstems of 7 fetuses (19 to 26 postconceptional weeks), and 10 infants (41 to 66 postconceptional weeks) without SIDS or neurological disease were analyzed. The brainstems of 1 child and 2 adults were also analyzed as indices of maturity for comparison. The median postmortem interval was 7 h (range: 2 to 24 h). There was no apparent

adverse effect of postmortem interval upon  $^3\text{H}$ -ligand binding in any region sampled, as found by others analyzing the same receptors in animal and adult human studies (e.g., 35,37). The relative distribution of radioligand binding to the selected receptors was essentially the same in either of the time periods examined, i.e., fetal period or early infancy, irrespective of the cause of death, agonal conditions, or postmortem interval; thus, the cases within each of these periods are described together. The high, intermediate, and low densities that we report in this study are relative to other regions within the brainstem, but not necessarily to forebrain regions.

#### *Distribution of Neurotransmitter Receptor Binding in the Human Infant ARC, nTS, and PGL*

The distribution of radioligand binding to the selected neurotransmitter receptors is illustrated at mid- and rostral levels of the medulla in a representative infant at 52 postconceptional weeks (Fig. 1). (As KA binding was not available in this case, it is illustrated from the medulla of a 47 postconceptional week infant.) In the infant ARC, muscarinic and KA binding was intense, and 5HT binding was low-to-moderate (Fig. 1). Relative to all other brainstem nuclei, muscarinic binding in the ARC was intermediate (100 to 200 fmol/mg), compared, for example, to high binding ( $>200$  fmol/mg) in the hypoglossal nucleus (Fig. 1) and other cranial nerve motor nuclei (39). Kainate binding was higher in the ARC ( $\geq 35$  fmol/mg) and the other rhombic-lip derivatives (inferior olive and basis pontis) than in any other brainstem site (40). Muscarinic, KA, and 5HT receptor binding colocalized precisely with the cytoarchitectonic boundaries of the ARC in individual sections. The ARC was not present in every section of the medulla sampled, nor was it of uniform density in every cell cluster or at every level throughout its caudorostral distribution. These observations are consistent with previous anatomic studies by us in which we found considerable variability within and among cases in the area and density of the ARC, including between serial sections separated by as little as 100  $\mu\text{m}$  (16,23). Of direct relevance to SIDS studies, this baseline variability mandates analysis in a sample of serial sections to establish significant differences in receptor binding in the ARC between SIDS and control cases.

Muscarinic, 5HT, and  $\alpha_2$  receptor binding was heavily concentrated in the infant nTS (Fig. 1). In contrast, KA receptor binding was low-to-moderate and nicotinic binding, negligible (Fig. 1). Throughout the infant nTS, the distribution of receptor binding for all of radioligands examined was heterogenous in both the cross-sectional and caudorostral plane. (The one exception was  $^3\text{H}$ -nicotine binding, which was negligible at all levels.)  $^3\text{H}$ -Naloxone binding to opioid receptors, for example, was twofold higher in the caudal than the mid-portion; rostrally it was high in the dorsolateral tegmentum, a region overlapping with and including the nTS (Fig. 1) (35). At the mid-level of the infant nTS, muscarinic, 5HT, and  $\alpha_2$ -receptor binding was heavily concentrated within

the dorsal subdivisions, with low or negligible binding in the ventral and ventrolateral subdivisions (Fig. 1). In the infant PGL, the binding was moderate (relative to other binding sites for the same radioligand within the same brainstem) for muscarinic and 5HT binding and or negligible for nicotinic, opioid, and KA binding (Fig. 1). In contrast,  $^3\text{H}$ -paraclonidine binding to  $\alpha_2$  receptors was high in the ventrolateral reticular formation of the rostral medulla, including regions that overlap with the cytoarchitectonic boundaries of the PGL (Fig. 1).

#### *Developmental Changes in Neurotransmitter Receptor Binding in the Human ARC, nTS, and PGL*

Receptor binding to all of the six radioligands analyzed was present and regionally distributed across the medullary nuclei by midgestation, the earliest time point examined. Over the last half of gestation, dramatic changes occurred in the relative distribution and quantitative levels of receptor binding densities in the ARC, nTS, and PGL. In the fetal ARC, as in the infant ARC, binding was negligible to nicotinic, opioid, and  $\alpha_2$  receptors and did not distinguish the ARC from the adjacent pyramid or other medullary surface structures (Table 3). In contrast, binding to both muscarinic and KA receptors in the ARC increased (by 63% and 49%, respectively) from midgestation to early infancy (Fig. 2), whereas binding to 5HT receptors decreased (by 40%) (Table 3). The elevations in muscarinic and KA binding appeared to be transient in the infant period, with a fall to adult levels at some point thereafter (Fig. 2).

In the nTS, binding to 5HT, nicotinic,  $\alpha_2$ , and muscarinic receptors decreased substantially from midgestation through early infancy, with the greatest decrease in 5HT and nicotinic binding (61% to 62%). In contrast, there were slight but not significant ( $<30\%$ ) decreases in binding to opioid and KA receptors (Table 3). In the PGL, binding decreased to varying degrees to all radioligands analyzed from midgestation to early infancy. The most substantial

**Table 3** Percent Change in Receptor Binding Between Midgestation and Infancy<sup>a</sup>

Receptor	nTS	PGL	ARC
5HT	↓62%	↓75%	↓40%
NIC	↓61%	↓73%	NM
$\alpha_2$	↓44%	↓85%	NM
MUS	↑38%	↑57%	↑63%
OPI	NS	↓58%	NM
KA	NS	↓34%	↑49%

<sup>a</sup>NS, not significant; NM, not measured due to visibly negligible binding in both fetal and infant periods.

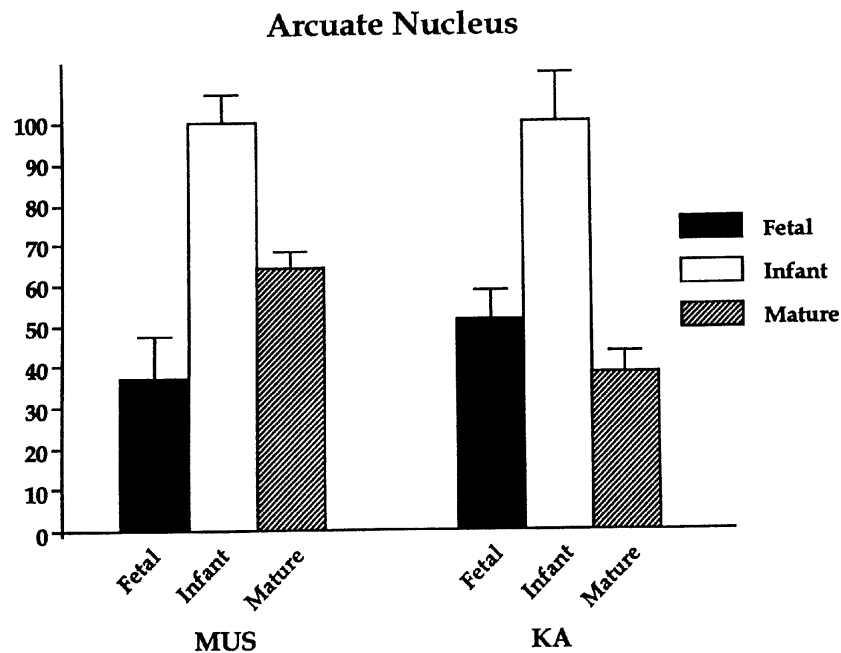


**Figure 2** A comparison of the percent changes ( $\pm$  SEM) in the development of  $^3\text{H}$ -QNB binding to muscarinic (MUS) receptors and  $^3\text{H}$ -kainate (KA) binding to KA receptors in the human ARC. Within each age group, there is a minimum of three cases (see text). One hundred percent was arbitrarily determined as the age group with the highest binding.

decrease occurred in  $\alpha_2$  binding (85%), and the least substantial, in KA binding (34%) (Table 3). While quench did increase in reticular subnuclei between the fetal and infant periods, the change was not significant, and correction for quench did not substantially change  $^3\text{H}$ -ligand binding levels in this data set (37). In contrast, there was a marked increase in quench in reticular subnuclei after early infancy to adult levels (37). In circumscribed nuclei that are not heavily intermixed with myelinated fibers, e.g., nTS, changes in lipid quenching between the fetal and infant periods were not substantial. Thus, the most dramatic quantitative changes between the fetal and infant periods of the nuclei sampled in this study were the decreases in  $\alpha_2$ , 5HT, and nicotinic binding in the PGL (Table 3), changes that were not fully explained by progressive myelination and lipid (myelin) quenching in the reticular formation.

### C. Discussion

Early human life is a critical period in the development of homeostatic control mechanisms, as the newborn adapts to independent life in the extrauterine environment (2). In the human fetus, diaphragmatic movements of breathing have

been demonstrated as early as 10 gestational weeks (57); at birth, respiration switches instantaneously from sporadic movements to a smooth, rhythmic pattern. The developmental timetable of central responses to  $\text{CO}_2$  in early human life is not completely known, but available data suggest that  $\text{CO}_2$  responsiveness develops preterm (50) and attains adult patterns at birth or very soon thereafter. From midgestation through early infancy, dramatic changes also occur in respiratory rate, state-dependent patterning, and responses to hypoxia (2,3). While the physiological changes in human respiration are fairly well described, very little is known about the underlying neuroanatomic and neurochemical development of the central controller sites. In this baseline autoradiography study of the human medulla, we examined the developmental profile of receptor binding to several neurotransmitters implicated in mediating or modulating cardioventilation across the critical period in autonomic and state maturation. We focused upon the ARC, a candidate VMS cell population for central chemoreception (23), as well as the nTS and PGL, two nuclei considered integral to the neuronal circuitry of central cardioventilatory control (9,47). While the development of this circuitry is complex and no single parameter underlies a particular physiological change, this autoradiographic study is a step toward defining the neurochemical maturation of the circuitry and is therefore of major relevance to SIDS analysis.

The localization of cholinergic, opioid,  $\alpha_2$ , KA, and 5HT receptor binding in the human infant nTS and PGL is consistent with animal physiological data showing the influence of the selected neurotransmitters upon cardioventilatory function via these nuclei (e.g., 35,43,44). Moreover, the receptors, cell bodies, and/or terminals of the selected neurotransmitters have been demonstrated within these two nuclei in experimental animals and/or adult humans (35,38,42-55). Our observations in the human infant nTS, for example, correlate well with those reported in the cat and rat nTS: anatomic studies in these species show a somatotopic organization of afferents within nTS subnuclei, and a regional distribution of opioid receptors and enkephalin-positive terminals (35). By analogy to animal data, the heterogeneous distribution of opioid receptors in the human infant nTS likely reflects a precise topography of cardioventilatory terminals: the heaviest concentration of opioid receptors occurs in the caudal subdivisions, which animal data link in part to baro- and chemoreflexes (35).

The prominent localization of muscarinic and KA receptor binding in the human infant ARC is consistent with animal data showing that these receptors play major roles in mediating the physiological responses of VMS cell populations (10,26,27,29,30,32-34). The experimental applications or microinjection of many neuroactive agents (cholinergic agonists, glutamate, KA, thyroid releasing hormone, substance P, and other neuropeptides) to the VMS results in dramatic effects on ventilation. They stimulate ventilation, while muscarinic antagonists, opiates, barbiturates, and GABA inhibit it (10,28,32,34), and clonidine decreases blood pressure (30). Yet, there is evidence that application of

